3D modelling in the Sado estuary using a new generic vertical discretization approach

Flávio MARTINS[a]*, Paulo LEITÃO[b], Adélio SILVA[c], Ramiro NEVES[b]

[a] Escola Superior de Tecnologia, Universidade do Algarve, Campus da Penha, 8000 Faro, Portugal

[b] Instituto Superior Técnico, Universidade Técnica de Lisboa, Portugal

[c] HIDROMOD Lda., Portugal

Abstract – Sado estuary (Portugal) is a mesotidal well-mixed estuary. The flow however, displays strong three-dimensional features associated with bathymetry variations. The flow is simulated using a three-dimensional primitive equation model based on the finite-volume method and incorporating a new concept for the vertical discretization. The innovative features of the model are analysed and the advantages of the finite-volume method to implement the generic vertical discretization are put into evidence. The model was validated using water level, velocity and salinity measurements in several stations along the estuary. Results show the influence of main channel's strong curvature on the generation of secondary flows inside the estuary. The steep bathymetry of the outer platform gives rise to a recirculation flow in the vertical plane that lasts for most of the tidal cycle. This structure is considered important for the sediment transport in that region. The above mentioned non-linear effects leave their print in both the transient and residual velocity fields. The results obtained help to understand the role of three-dimensional structures on the water exchange and sediment transport in the estuary. The results also confirm the suitability of the approach used in this model to simulate estuarine and coastal flows with strong three-dimensional effects. © 2001 Ifremer/CNRS/IRD/Éditions scientifiques et médicales Elsevier SAS

Résumé – Modélisation 3D dans l'estuaire du Sado avec une nouvelle approche par discrétisation verticale générique. Ĺestuaire du Sado (Portugal) est brassé par une marée méso-échelle, mais Íécoulement y présente des aspects tridimensionnels. La simulation utilise un modèle aux équations primitives, basé sur la méthode des volumes finis avec un nouveau concept de discrétisation verticale. Les caractéristiques du modèle sont analysées et les avantages de la méthode des volumes finis sont mis en évidence. Le modèle a été validé en utilisant des hauteurs d'eau, des vitesses et salinités mesurées en plusieurs stations au long de l'estuaire. Les résultats montrent le rôle de la forte courbure du chenal principal dans la formation d'écoulements secondaires dans l'estuaire. La bathymétrie abrupte de la plate-forme externe induit une remise en circulation dans le plan vertical qui s'étend sur la presque totalité d'un cycle de marée. Cette structure est importante dans le transport sédimentaire. Les effets non-linéaires sont visibles sur les champs de vitesse résiduelle et transitoire. Les résultats permettent de comprendre le rôle des structures tridimensionnelles dans les échanges de masses d'eau et le transport de sédiment dans l'estuaire. Ils confirment la pertinence de l'approche utilisée

*Correspondence and reprints.
E-mail addresses: fmartins@ualg.pt (F. MARTINS), chambel@hidro1.ist.utl.pt (P. LEITÃO), asilva.hidromod@taguspark.pt (A. SILVA), ramiro.neves@hidrox.ist.utl.pt (R. NEVES).

pour simuler les écoulements côtiers et estuariens où les effets tridimensionnels sont importants. © 2001 Ifremer/CNRS/IRD/Éditions scientifiques et médicales Elsevier SAS

estuaries / numerical modelling / secondary flows / vertical recirculation / generic vertical discretization

estuaires / modélisation numérique / écoulements secondaires / recirculation verticale / discrétisation verticale générique

1. INTRODUCTION

During the last two decades, advances achieved in both data measurement and modelling enabled the identification of the principal 3D features present in marine environments. First-order effects are well understood and can be accurately modelled. Attention is nowadays moving to non-linear interactions and to second-order effects. Simulation of these processes requires increasingly fine resolution both in horizontal and vertical directions. To maintain affordable simulation times, methods to describe vertical distributions and transport must be improved. In this paper a three-dimensional primitive equations model is presented. The model implements a new generic vertical discretization approach using the finite volume method. This approach is used to simulate the three-dimensional characteristics of the flow in Sado estuary.

Sado estuary is located 40 km south of Lisbon, Portugal, as shown in *figure 1*. It is about 20 km long and 4 km wide. The maximum depth is larger than 50 m and average depth is about 8 m. The estuary displays strong curvature and intertidal sandbanks individualise a northern and a southern channel. In the upper reaches intertidal mudflats and salt marshes occupy about one third of the estuary.

The tide is semidiurnal, with an amplitude of about 1.6 m in spring tides, and 0.6 in neap tides. The most important tidal components are M2 and S2. At the mouth their amplitudes are 0.98 m and 0.35 m respectively, both being amplified inside the estuary. The river flow displays a strong seasonal variability. In summer, monthly average values lower than $1 \, m^3 \cdot s^{-1}$ are observed, while during winter average values of $60 \, m^3 \cdot s^{-1}$ are usual.

The ecological and economical importance of the estuary is at the origin of the studies carried out. Bathymetric data is measured periodically, mainly in the navigation area. Tides and currents have been measured by Sobral (1977) in a few points in the estuary using fixed instruments.
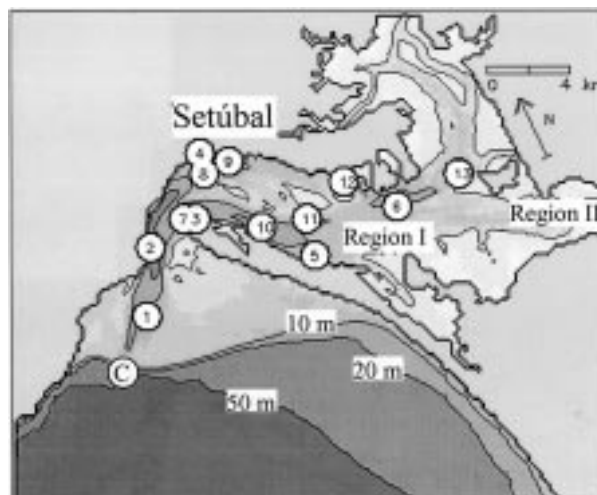
Figure 1. Sado estuary bathymetry and field stations.

Ribeiro and Neves (1982) measured velocities in 12 fixed stations during complete tidal cycles and horizontal distributions of salinity and temperature. Wollast (1978; 1979) measured hydrological and geochemical properties. These studies highlighted the main processes controlling the circulation in the estuary and gave a first idea of its environmental state. The flow is mainly tidally driven and very strong residual eddies exist inside the estuary associated with the curvature of the main channels. The lower estuary is occupied by two major eddies, while in the upper estuary the residual flow is more complex. This circulation supports the subdivision of the estuary in its upper and lower part as suggested by Wollast (1979), based on the temperature and salinity distributions. The lower estuary behaves as a coastal lagoon with small fresh water influence, while the upper reaches of the estuary present a riverine behaviour. More recently, studies involving sediment transport have been carried out (Rodrigues, 1992 ; Vale and Sundby, 1987). Again these studies showed the difference between the

upper and lower estuary and put into evidence the importance of three-dimensional circulation, to explain their data.

A navigation channel 14-m deep is dredged across the outer region of the estuary. In this region a sharp depth gradient connects the estuary to the platform. Due to this complex geometry it is expected that only a 3D model will be able to simulate realistically the flow in the region. A full 3D model was applied to access the role of the vertical velocity field and secondary flows in the hydro-dynamics of the estuary. Due to the weak river flow rate, baroclinic effects are not expected to be important. For that reason the simulations were conducted only in barotropic mode.

2. THE VERTICAL DISCRETIZATION

In shallow areas topographic features play a major role controlling the flow, while in the deep ocean the density field is a major driving force. Sigma-type coordinates (Philipps, 1957) optimize topographic representation, allowing the same number of grid points for every depth. This discretization is quite advantageous for the simulation of barotropic flows because the flow closely follows gridlines and the vertical advective exchanges between cells are minimized. When a clear thermocline is present and a nearly horizontal mixing layer exists, the flow does not follow the bottom topography and the usual sigma coordinate produces ill-behaved results. Since in most situations the thermocline is close to horizontal, some authors use a double sigma coordinate, splitting the water column into an upper nearly horizontal and a lower terrain following sub-domains (Deleersnijder and Beckers, 1992 ; Santos, 1995). Isopycnic coordinate models use the density as the vertical coordinate (Oberhuber, 1993 ; Bleck and Boudra, 1986). As a consequence, the mesh is aligned with constant density lines. Longitudinal transport plus a grid deformation represent most advection. These models can thus minimize numerical diffusion and preserve water mass properties when the flow is fully governed by density gradients, but are not adequate to study barotropic flows or whenever topography plays a major role in the flow. Cartesian coordinate models are a compromise between former types (Bryan, 1969). There is no optimization, but the model can be used in every domain if enough computational power is available.

In real domains the relative importance of topographical effect, density forcing, inertia, and diffusion is different from point to point and therefore there is no unique optimal vertical coordinate for the whole domain. Instead, different discretizations should be implemented for different regions. In such a generic discretization approach the model must be able to solve the governing equations in a grid with any kind of geometry. This can be achieved in two different ways. The differential equations can be transformed using a generic transformation and the actual form of the grid controlled by the transformation Jacobean in each grid location (Deleersnijder and Ruddick, 1992). An alternative approach is to define explicitly the geometry of the grid and use a method suitable to solve the equations directly on that grid. One of the advantages of this approach is that any law, regardless of the Jacobean complexity that it produces, can be used to impose the grid geometry.

Most circulation models are based on finite-difference or finite-element methods. A less popular method is the finite volume approximation (Chippada et al., 1998). In this approach the discrete form of the governing equations are applied macroscopically to the cell control volume. The grid is therefore defined explicitly and the equations solved by the same procedures irrespectively of the cell geometry. Since the equations are solved in the form of flux divergences this method automatically guarantees the conservation of transported properties (Ferziger and Perić, 1995 ; Vinokur, 1989).

In this paper a new primitive equations model using the finite volume method is used to simulate the three-dimensional characteristics of the flow in Sado estuary. The model solves the equations in the real domain without any space transformation. The geometry information is carried in the areas and volumes needed to calculate the fluxes. In this way, a complete separation between the hydrodynamic variables and the geometry is accomplished for all mesh types. The geometry information is updated in each time step as a function of the mesh type. The computational effort necessary to do this is comparable to that used in solving the Jacobean of the transformation, and the method is much more flexible (Vinokur, 1989). The cells can have any initial shape and suffer any time deformation. This flexible architecture is equivalent to a generic vertical co-ordinate. The same code can be used with every discretization and different discretizations can be used simultaneously in different regions of the domain (Martins et al., 1998).
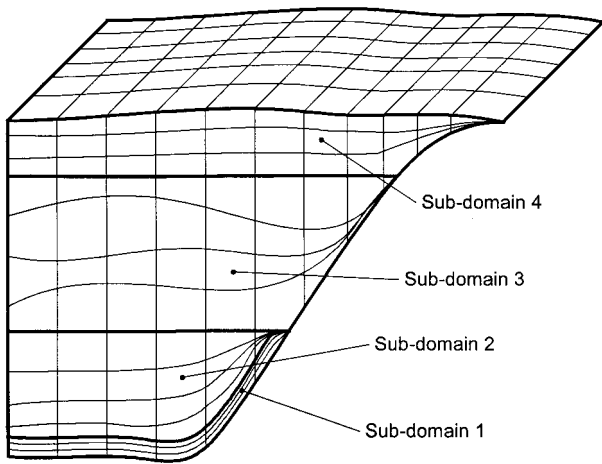
Figure 2. Domain decomposition enabling a different grid law for each sub-doma.

In this model the domain can be divided vertically into sub-domains and a different grid law can be applied explicitly to each sub-domain as depicted in *figure 2*. The computational cells have some restrictions on their geometry in order to alleviate the storage and computational requirements of the model. The vertices have only one degree of freedom, along the vertical direction, being fixed in the horizontal plane as depicted in *figure 3*. The U_i velocity cells are staggered in an Arakawa-C manner (Arakawa and Lamb, 1977).
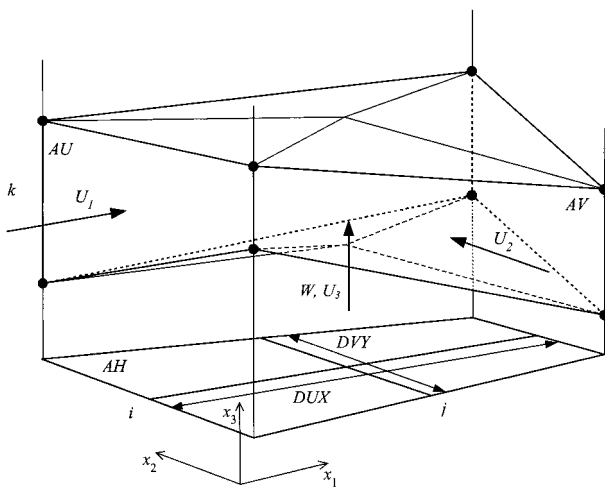

Figure 3. Cell geometry and nomenclature.

3. SOLUTION OF THE GOVERNING EQUATIONS

The model solves the three-dimensional primitive equations in Cartesian coordinates for incompressible flows. Hydrostatic equilibrium is assumed, as well as Boussinesq approximation. The mass and momentum evolution equations are:

$$\frac{\partial u_i}{\partial x_i} = 0 \tag{1}$$

$$\frac{\partial u_1}{\partial t} + \frac{\partial (u_j u_1)}{\partial x_j} = -fu_2 - g\frac{\rho_\eta}{\rho_0}\frac{\partial \eta}{\partial x_1}$$
$$-\frac{1}{\rho_0}\frac{\partial p_s}{\partial x_1} - \frac{g}{\rho_0}\int_z^\eta \frac{\partial \rho'}{\partial x_1}dx_3 + \frac{\partial}{\partial x_j}\left(A_j\frac{\partial u_1}{\partial x_j}\right) \tag{2}$$

$$\frac{\partial u_2}{\partial t} + \frac{\partial (u_j u_2)}{\partial x_j} = fu_2 - g\frac{\rho_\eta}{\rho_0}\frac{\partial \eta}{\partial x_2} - \frac{1}{\rho_0}\frac{\partial p_s}{\partial x_2}$$
$$-\frac{g}{\rho_0}\int_z^\eta \frac{\partial \rho'}{\partial x_2}dx_3 + \frac{\partial}{\partial x_j}\left(A_j\frac{\partial u_2}{\partial x_j}\right) \tag{3}$$

$$\frac{\partial p}{\partial x_3} = -\rho g \tag{4}$$

Where u_i are the velocity vector components in the Cartesian x_i directions, η is the free surface elevation, f the Coriolis parameter, A_i the turbulent viscosity and p_s is the atmospheric pressure. ϱ is the density and ϱ' its anomaly. The density is calculated as a function of temperature and salinity by the equation of state (Leendertse and Liu, 1978):

$$\rho = (5890 + 38T - 0.375T^2 + 3S)$$
$$/[(1779.5 + 11.25T - 0.0745T^2) - (3.8 + 0.01T)S +$$
$$0.698(5890 + 38T - 0.375T^2 + 3S)] \tag{5}$$

The computed flow field transports salinity, temperature and any other tracer using an advection-diffusion equation.

The model uses a semi-implicit ADI algorithm with two time levels per iteration. Two numerical schemes are currently implemented: the four equations S21 scheme (Abbot et al., 1973) and the six equations Leendertse scheme (Leendertse, 1967). The time discretizations for these numerical schemes are depicted in *figures 4* and *5* respectively.
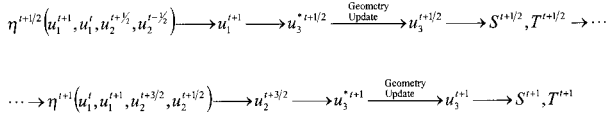
$$\eta^{t+1/2}\left(u_1^{t+1}, u_1^t, u_2^{t+1/2}, u_2^{t-1/2}\right) \longrightarrow u_1^{t+1} \longrightarrow u_3^{\bullet t+1/2} \xrightarrow[\text{Update}]{\text{Geometry}} u_3^{t+1/2} \longrightarrow S^{t+1/2}, T^{t+1/2} \rightarrow \cdots$$

$$\cdots \rightarrow \eta^{t+1}\left(u_1^t, u_1^{t+1}, u_2^{t+3/2}, u_2^{t+1/2}\right) \longrightarrow u_2^{t+3/2} \longrightarrow u_3^{\bullet t+1} \xrightarrow[\text{Update}]{\text{Geometry}} u_3^{t+1} \longrightarrow S^{t+1}, T^{t+1}$$

Figure 4. Time discretization of the S21 numerical scheme.

The free surface elevation is computed through integration of equation 1 over the water column. The two components of the horizontal velocity are globally centred in *t+1/2* leading to a second order time accuracy (Martins et al., 1998). Vertical fluxes are also computed by continuity (hydrostatic approach), integrating over each cell volume. Since the mesh is allowed to move along the vertical direction the computation of the vertical fluxes and the redefinition of the geometry are calculated in conjunction. This process is analysed in the next sections.

3.1. Discretization of the momentum equations

The momentum equations are integrated for each cell volume *i,j,k*. The time derivative term must be integrated over the control volume that is also variable in time. This can be easily done with the aid of the Leibnitz rule that, for volume integrals read:

$$\frac{\partial}{\partial t}\int_V f\, dV = \int_V \frac{\partial f}{\partial t}\, dV + \int f(\vec{v}_s \cdot \vec{n})\, dS \qquad (6)$$

where *S* is the cell surface, *V* the volume, $\vec{n}$ the outward normal and $\vec{v}_s$ is the velocity of that surface relative to a fixed referential. The integration of the first term of equation 2:

$$\int_{V_{uij}} \frac{\partial u_i}{\partial t}\, dV = \frac{\partial}{\partial t}\int_{V_{uij}} u_i\, dV - \int_{sc} u_i(\vec{v}_s \cdot \vec{n})\, ds \qquad (7)$$

$$u_2^{t+1/2} \longrightarrow \eta^{t+1/2}\left(u_1^{t+1/2}, u_2^t\right) \longrightarrow u_1^{t+1/2} \longrightarrow u_3^{\bullet t+1/2} \xrightarrow[\text{Update}]{\text{Geometry}} u_3^{' t+1/2} \longrightarrow S^{t+1/2}, T^{t+1/2} \rightarrow \cdots$$

$$\cdots \rightarrow u_1^{t+1} \longrightarrow \eta^{t+1}\left(u_1^{t+1/2}, u_2^{t+1}\right) \longrightarrow u_2^{t+1} \longrightarrow u_3^{\bullet t+1} \xrightarrow[\text{Update}]{\text{Geometry}} w_3^{t+1} \longrightarrow S^{t+1}, T^{t+1}$$
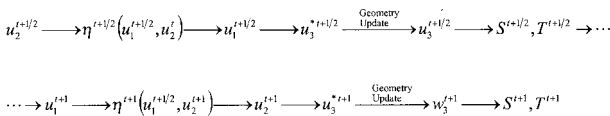
Figure 5. Time discretization of the Leendertse numerical scheme.

is approximated as:

$$\frac{U_i^{t+1} \cdot V_u - U_i^t \cdot V_u}{\Delta t}$$
$$- \left[(U_i \cdot W_s \cdot A_{H_{ij}})_{top} - (U_i \cdot W_s \cdot A_{H_{ij}})_{bot} \right] \qquad (8)$$

where U_i(considered constant over each cell face) is the discretized velocity component in the Cartesian referential, V_u is the volume of the u-cell and *sc* it's boundary surface. In the last term A_H is the projected area of the top and bottom cell faces into the horizontal plan. W_s is the velocity of those faces and is determined by the vertical movement of the vertices as a function of the particular grid law in use. The other terms of the surface integral are not present since the cell adopted in this model do not admit horizontal movement of the lateral faces.

The advective term of equation 2 is integrated with the aid of the Gauss theorem, applied to the volume in some instant of time between *t* and *t+1*:

$$\int_{V_{ij}} div(u_i \vec{v})\, dV = \int_{Sc} u_i \vec{v} \cdot \vec{n}\, dS \qquad (9)$$

This term is approximated as:

$$(U_i\, U1flux)_{ij+1} - (U_1\, U1flux)_{ij} + (U_1\, U2flux)_{i+1j}$$
$$- (U_i\, U2flux)_{ij} + (U_i\, WA_{H_{ij}})_{top} - (U_i\, WA_{H_{ij}})_{bot} \qquad (10)$$

were *Uiflux* are the horizontal water fluxes across the U cell faces and *W* is the absolute vertical velocity. The last terms of equations 8 and 10 can be added producing:

$$[U_i \cdot (W - W_{s+}) \cdot A_{H_{i,j}}]_{top} - [U_i \cdot (W - W_s) \cdot A_{H_{i,j}}]_{bot}$$
$$= (U_i \cdot Wr \cdot A_{H_{i,j}})_{top} - (U_i \cdot Wr \cdot A_{H_{i,j}})_{bot} \qquad (11)$$

where *Wr* is the vertical velocity of the fluid measured relative to the top and bottom surfaces and $W_r\, A_H = U3flux$ is the water flux trough that surface. This term can be viewed as the advective fluxes entering the moving cell. The particular discretization of this advective term depends on the advective method used. The final form of the u_i momentum equation is:

$$\frac{V_u(U_i^{t+1} - U_i^t)}{\Delta t} + \sum_j U_i \cdot Ujflux = \frac{1}{\rho_0}F_i \qquad (12)$$

F_i is the x_i component of the forces applied to the fluid mass due to barotropic, baroclinic, Coriolis, horizontal and vertical diffusion effects. Since the lateral cell faces are vertical, the fluxes through those faces are completely

horizontal. The advective and diffusion terms however are iso-layer operators. This can lead to artificial vertical transport in sloping meshes but are preferable in bathymetry influenced regions since the bottom processes are not destroyed (Mellor and Blumberg, 1985).

For stability reasons the vertical transport and barotropic pressure are computed implicitly, all the other terms in equation 12 are calculated explicitly.

For some grid laws the volume V_u is dependent on the hydrodynamic variables and is not known at the instant *t+1* during the calculation of the horizontal velocities. For this reason the geometry changes are taken into account during the computation of the vertical velocities.

3.2. Processes in the vertical direction

The vertical velocity in each cell is calculated by continuity integrating equation 1 in the cell volume and in time. The surface integral extends to all cell faces and the horizontal fluxes used in this equation must be the same used in the momentum and elevation equations in order to ensure conservation.

The cell volume at *(t+1/2)* depends on the vertical discretization in use: For sigma discretization the volume is a function of time through η and can be readily calculated. For isopycnic discretization the mesh moves as a function of the density field that have not been calculated yet, finally for the lagrangean discretization the mesh moves as a function of the vertical velocity itself and the procedure should be implicit.

In order to implement a generic discretization method the vertical velocity is computed in two steps. In the first step the value Wr^* is predicted assuming that the volume remains constant:

$$A_{H_{ij}} \cdot (Wr^{*t + 1/2}_{ijk + 1} - Wr^{*t + 1/2}_{ijk}) = \sum_j Ujflux \quad (13)$$

The Wr^* value is then used, if needed, for the redefinition of the mesh geometry. The value of the vertical velocity is then corrected using the volume variation:

$$A_{H_{ij}} \cdot (Wr^{t + 1/2}_{ijk + 1} - Wr^{t + 1/2}_{ijk}) = \sum_j Ujflux - \frac{Vol^{t + 1/2}_{ijk} - Vol^{t}_{ijk}}{\Delta t/2} \quad (14)$$

3.3. Boundary conditions

Five types of boundaries were used in this application: free surface, bottom, lateral closed boundary, lateral opened boundary, and moving boundary.

At the free-surface boundary the water flux across the surface was assumed null

$$Wflux|_{sup} = 0 \quad (15)$$

and the wind stress was not considered.

At the bottom boundary the water flux is also assumed null and a quadratic law is used to calculate the bottom stress:

$$v_3 \frac{\partial u_i}{\partial x_3}\bigg|_{bot} = C_D u_i \sqrt{u_1^2 + u_2^2} \quad i = 1,2 \quad (16)$$

Were v_3 is the vertical eddy viscosity and C_D is the drag coefficient. For stability reasons the bottom stress must be calculated implicitly in the momentum equation of the bottom cell. This is accomplished using a procedure proposed by Backhaus (1983).

The closed boundaries of the domain correspond to land. The area of that surface is much smaller than the bottom surface. Also, the horizontal resolution of this mesoscale model is larger than the characteristic dimension of the lateral boundary layer. For that reasons an impermeable, free slip condition was adopted:

$$\frac{\partial u_1}{\partial x_2} = \frac{\partial u_2}{\partial x_1} = 0 \quad (17)$$

$$u_i \cdot n_i = 0 \quad (18)$$

Using the finite volume method this is accomplished in a direct way specifying zero water fluxes and zero momentum diffusive fluxes for the cell faces in contact with land.

At the open boundaries the tidal signal was imposed specifying the free surface elevation of that cells.

Moving boundaries are closed boundaries whose position varies with time; this type of situation arises in domains with inter-tidal zones. In this case the uncovered cells must be tracked. For computational reasons the condition η ≤ –h, h being the local depth, cannot be used to decide if a cell is uncovered. Instead, a criteria based on *figure 6* is used. HMIN is the depth below which the
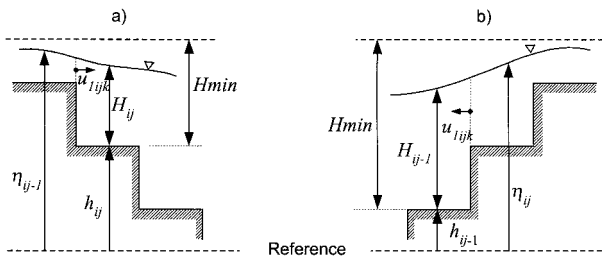
Figure 6. Conditions for uncovered cells.

Figure 7. Water level time series in station 6.

cell is considered uncovered; thus conserving a thin sheet of water above the uncovered cell. The cells of position i,j are considered uncovered when at least one of the two following situations is true:

$$H_{ij} < HMIN \quad and \quad \eta_{ij-1} < -h_{ij} + HMIN \qquad (19)$$

or

$$H_{ij-1} < HMIN \quad and \quad \eta_{ij} < -h_{ij-1} + HMIN \qquad (20)$$

Where $H = h + \eta$ is the total depth. The second condition of equation 19 assures that the cell is not being covered by waves propagating from the left to the right and the second condition of equation 20 assures that the cell is not being covered by waves propagating from the right to the left. The noise formed by the abrupt variations in velocity of the dry cells is controlled with a careful choice of HMIN (Leendertse and Liu, 1978).

4. RESULTS

The model was used in Sado estuary to characterize the three-dimensional features of the flow present in some regions of the domain. Because in summer the river flow is small, a barotropic simulation was carried out. A 120×158 points horizontal mesh with 200 m constant horizontal step was used. The model was coupled to a 1D model for the river section of the estuary. This 1D model solves the same set of equations of the complete 3D model. The same code is in fact used in both cases, since the model can be run in 1D, 2D or 3D mode. Vertical discretization was based on a sigma grid law with six layers, except for the recirculation analysis where other mesh configurations were used.
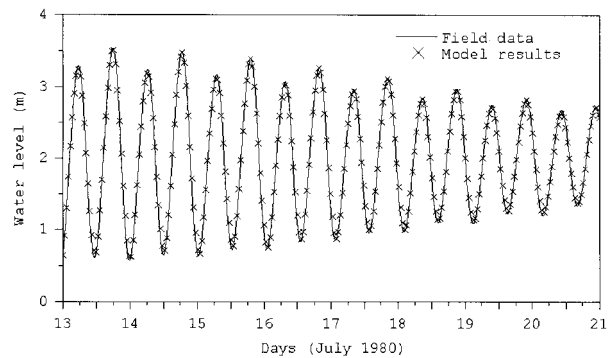
4.1. Model calibration

Tidal height and velocity measurements were used to calibrate the model. The water level was imposed at the sea boundary using 22 harmonic constants from the Sesimbra tide gauge (Sobral, 1977). For the river flow daily averages were imposed. During the simulation period the flow varied from a minimum of 1.1 m^3s^{-1} to a maximum of 1.4 m^3s^{-1}. The paper industry is also the origin of fresh water that must be considered. For that effluent a monthly average of 0.19 m^3s^{-1} was used. The urban effluent and non-point sources were very low and were not considered. The wind stress was also not considered since the variability was very high.

4.1.1. Hydrodynamic calibration

The model results were compared with field data at six water level stations (1 to 6 in *figure 1*) and seven velocity stations (7 to 13). Each velocity station comprises a current meter located 1 m below the surface and another one located 3 m above the bottom (Ribeiro and Neves, 1982). In *figure 7* the water level data of station 6, located in the interior of the estuary is compared with model results for the period 13–21 July. The agreement is quite good with maximum errors less than 1%.

Velocity values from the model were also compared with field data. In *figure 8* field data and model results are compared for station 11. Since only short period velocity records were available it was not possible to decompose the data into their constituents. Instead, the raw data were used in this comparison. There is satisfactory agreement both for water slack instants and velocity values.
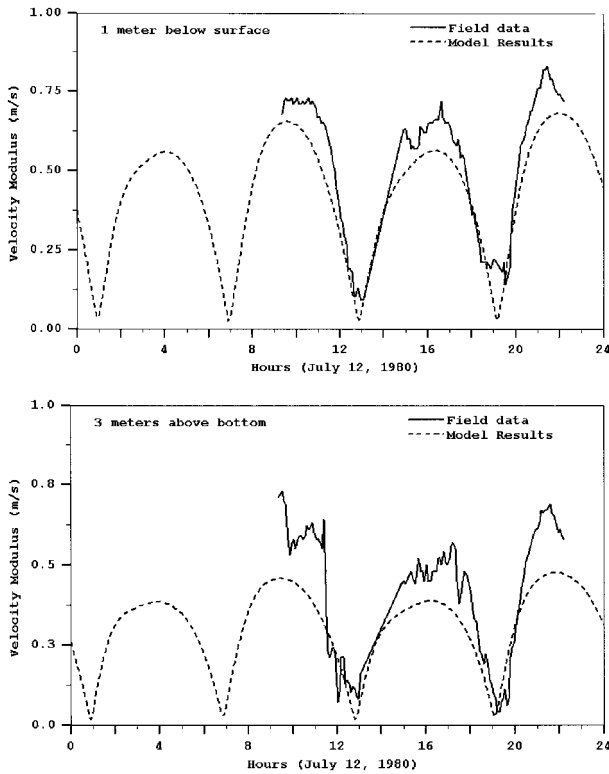
Figure 8. Velocity modulus time series in station 11.

Figure 9. Vertical recirculation in a steep region, sensibility to vertical viscosity.

4.2. Three-dimensional effects

A region of steep bathymetry makes the transition between the estuary and the coastal waters. The maximum gradient found in this region is about 1/10. A pronounced slope like this can produce recirculation flows in the vertical plan during the ebb period. If the momentum is high in the top layers the increase in depth will produce a large positive pressure gradient in the direction of the flow. The shield effect produced by the slope induces a momentum deficit in the base of the slope. Due to this lack of momentum, the flow in that region cannot withstand the pressure gradient and reverse its direction. In *figure 9* the transient velocity field in a vertical cut through that region is presented. The cut location is indicated by point C in *figure 1*. The recirculation can be identified during almost 3 h of the ebb period.

The recirculation only exists if the high momentum of the top layers cannot be efficiently transported to the lower layers. Since this transport is mainly diffusive the recirculation must be very sensitive to the vertical diffusion of
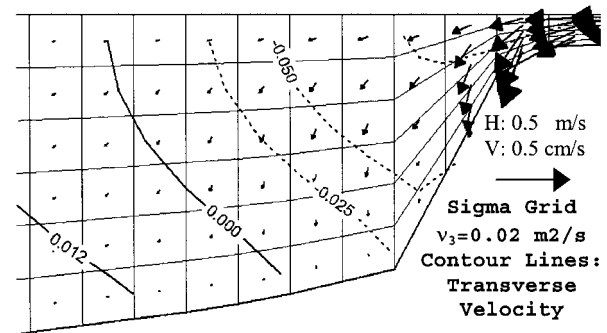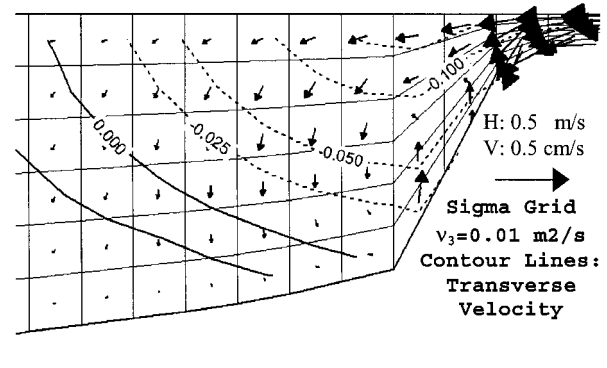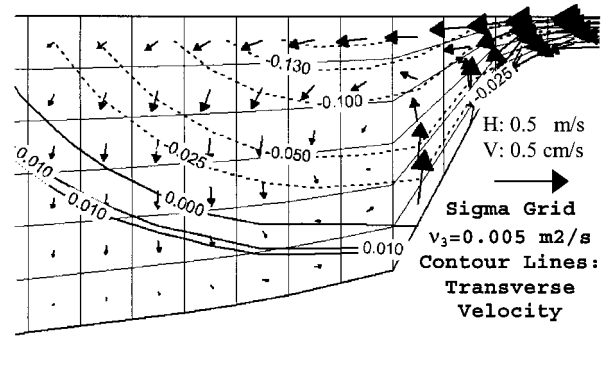
momentum. In the numerical results this diffusion is produced not only by the diffusive term but also by the numerical diffusion created by the model. The numerical diffusion depends on the numerical discretization of the non-linear terms and is also a function of the flow direction relative to the mesh. For that reason the grid geometry will influence the existence and size of the recirculation.

8

A sensibility analysis was performed to investigate the influence of the vertical eddy viscosity coefficient and grid geometry on the recirculation characteristics.

Figure 9 show the flow in the cut region 4 h after high waters for vertical viscosity values of $0.005 \text{ m}^2\text{s}^{-1}$, $0.01 \text{ m}^2\text{s}^{-1}$, and $0.02 \text{ m}^2\text{s}^{-1}$. Six equally spaced sigma layers were used. It can be seen that the recirculation is highly sensitive to the vertical diffusion not appearing at all for the $0.02 \text{ m}^2\text{s}^{-1}$ run.

The influence of different mesh discretizations upon the formation and size of the recirculation was also analysed. Using the generic vertical discretization approach described above, three different meshes were tested: Sigma, Cartesian and Lagrangean, as depicted in *figure 10*. In all cases a vertical viscosity of $0.01 \text{ m}^2\text{s}^{-1}$ was used. The Cartesian discretization used was of the shaved cell type (Adcroft et al., 1997). In this discretization, cells with cuts in the regions where they intersect the bathymetry represent the bottom topography. The Lagrangean discretization is based on an original sigma mesh. In each time step the mesh is allowed to perform controlled displacements from its original geometry, based on the local vertical velocity.

With the Cartesian discretization the flow exhibits excessive diffusion, and the recirculation cannot be correctly represented if the same number of layers is used. This diffusive behaviour is attributed to numerical diffusion due to the large angle between the velocity field and the mesh principal directions. Both the sigma and the Lagrangean discretizations reduce this angle producing a more identified vortex.

4.3. Residual currents

The residual velocity field helps the understanding of long-term water exchange inside the estuary and is a valuable tool to comprehend its sediment dynamics. For that reason the residual flow for a nine days period was computed. Six sigma layers were used and the calibrated (constant) vertical viscosity of $0.01 \text{ m}^2\text{s}^{-1}$ was applied. This value was also used as the reference case for the sensibility analysis. In *figure 11* the residual velocity field for the surface layer can be seen. Two residual circulation structures in the horizontal plan can be identified near the mouth and a clockwise eddy in the interior of the estuary. Along the main channel a strong transport towards the
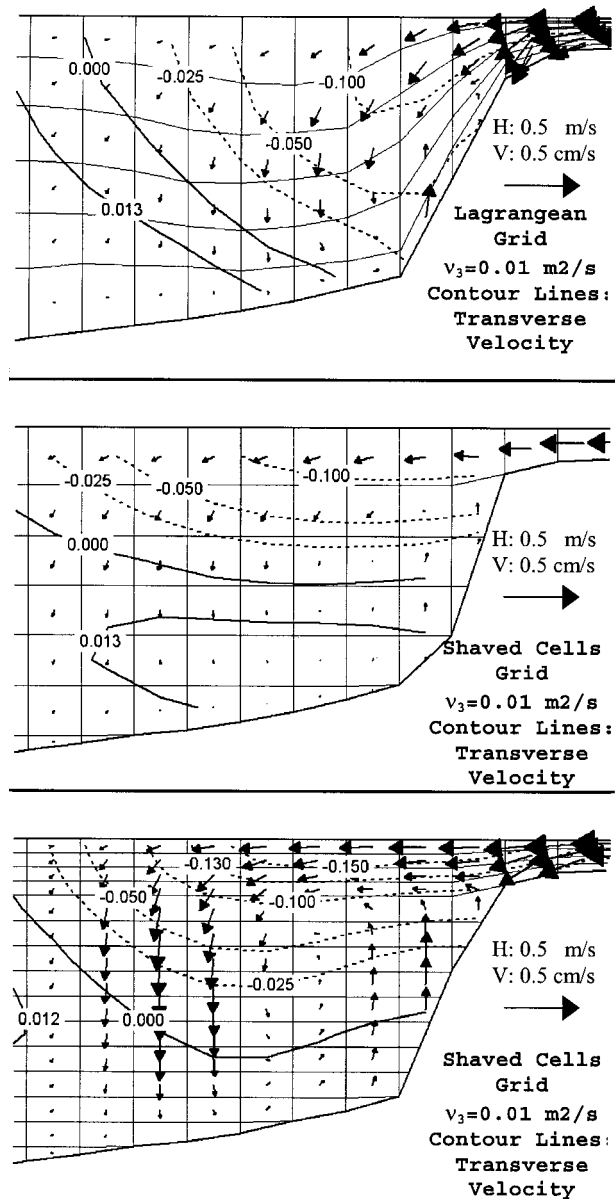

Figure 10. Vertical recirculation in a steep region, sensibility to grid geometry.

ocean is also present. In *figure 12* a vertical cut through the inlet region is presented. This residual secondary flow shows a NW surface transport from the sandbank to the main channel and a SE bottom transport. Based on those figures, a mechanism explaining the stability of the sandbank southeast from station 2 and the deep bathymetry of the inlet can be suggested. The surface horizontal
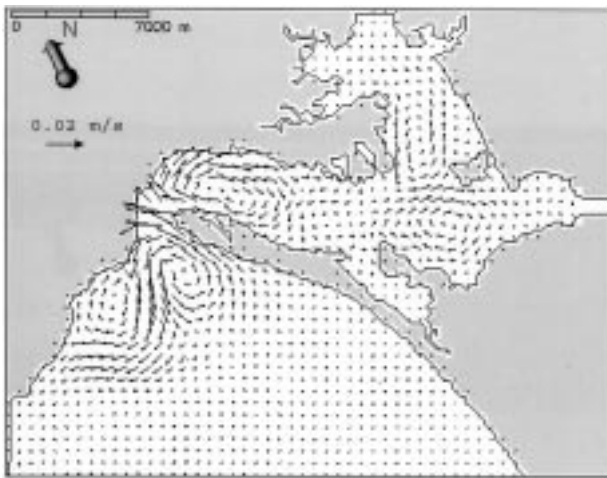
Figure 11. Residual circulation of the top layer.

eddy recirculates the sediments that have exited the estuary towards the sandbank. The secondary flow of *figure 12* feeds them to the slope. Since this process occurs on the outside of the estuary the low frequency residual flows suffer influence from higher frequency mechanisms such as wind waves. Further research must therefore be developed to evaluate the relative importance of each process.

Inside the estuary the average wind activity is rather low making this type of analysis more reliable. The sandbanks between the north and south channels, in the estuary interior, receive their sediment supply mainly from riv-
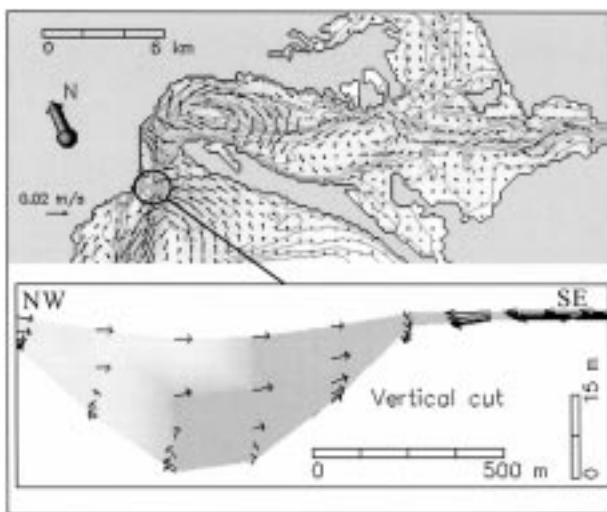

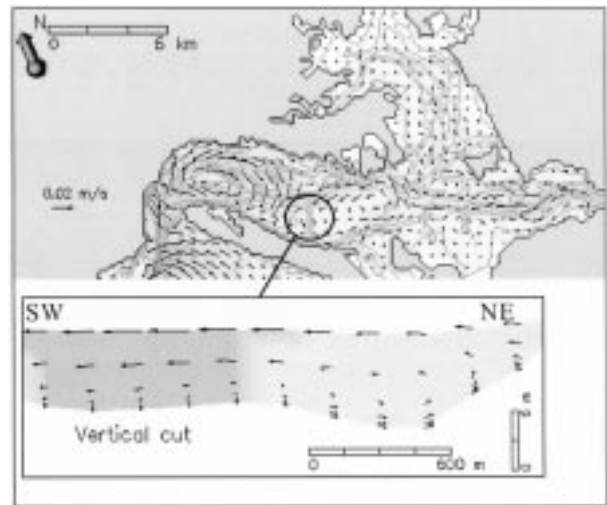**Figure 12.** Residual vertical circulation in the main channel.

Figure 13. Residual vertical circulation in the south channel.

erine sources. The horizontal residual circulation is expected to play a major role in the distribution of sediments to the sandbanks. A mechanism similar to the one described above is proposed to explain the stability of these sandbanks. *Figure 13* shows a surface transport associated with the horizontal recirculation that delivers sediments to the channel, and a bottom transport that feeds back the sediment to the sandbank. The sediments from the south channel are forced to the north channel by the horizontal circulation. In *figure 14* a vertical cut of the north channel show a bottom transport towards the sandbank capable of maintain the equilibrium with the surface transport towards the channel.

These strictly hydrodynamic results show the importance of an accurate three-dimensional simulation to obtain good results from sediment transport models. This is frequently neglected in barotropic situations, and can lead to large inaccuracies in bathymetries with strong curvature.

5. CONCLUSIONS

The 3D effects in the Sado estuary have been shown as very important even in barotropic conditions. Regions of strong vertical velocities producing recirculation on the vertical plane where identified. These flows are associated with curvature of the channels and with bathymetry variations. Simulations using Cartesian, sigma and
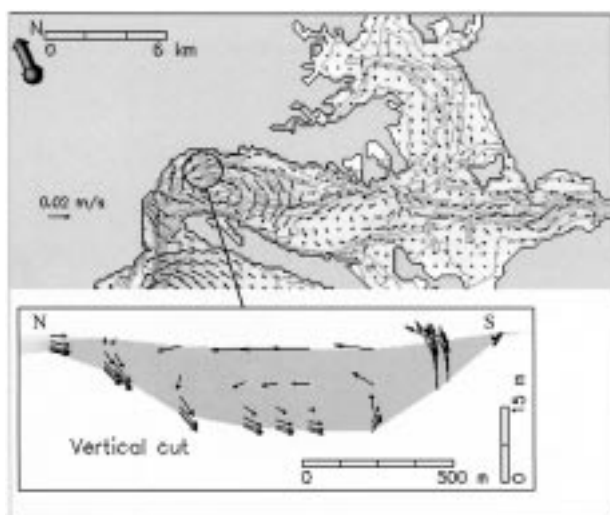
Figure 14. Residual vertical circulation in the north channel.

Lagrangean meshes were performed to access the sensibility of the results to different vertical discretizations. Differences between the results were illustrated comparing the vertical recirculation at the outlet. Sigma and Lagrangean meshes give similar results. To obtain the recirculation vortex using the Cartesian mesh, a bigger number of layers was necessary.

Despite these differences, the tendency to recirculate was consistent for every mesh and for every viscosity value. This enabled a qualitative interpretation of three-dimensional hydrodynamic features' effects upon the sediment dynamics of the estuary. In this interpretation the sand banks forming the northern and southern channels are shown to originate from residual circulations on the vertical plane, associated with the curvature of the estuary. It is also shown that the vertical recirculation during the ebb in the slope adjacent to the exterior platform can contribute to build and maintain that slope.

The Lagrangean discretization used in the sensitivity analysis was initialised with a sigma mesh and allows controlled displacements that tend to align it with the velocity field. Numerical diffusion is expected to be smaller producing better results, although the differences are small. Lagrangean grid is expected to improve model results in baroclinic flows, especially in the presence of internal waves, which can create large numerical diffusion when simulated by a small number of fixed layers.

6. UNCITED REFERENCES

This section comprises references that occur in the reference list but not in the body of the text. Please position each reference in the text or, alternatively, delete it. Any reference not dealt with will be retained in this section: Levitus, 1982 ; Neves, 1985.

REFERENCES

Abbot, M.B., Damsgaardand, A., Rodenhuis, G.S., 1973. System 21, Jupiter, a design system for two-dimensional nearly-horizontal flows. J. Hyd. Res. 1, 1–28.

Adcroft, A.J., Hill, C.N., Marshall, J., 1997. Representation of topography by shaved cells in a height coordinate ocean model. Mon. Weather Rev. 125, 2293–2315.

Arakawa, A., Lamb, V., 1977. Computational design of the basic dynamical processes of the UCLA general circulation model. Meth. Comput. Phys. 17, 174–267.

Backhaus, J., 1983. A semi-implicit scheme for the shallow water equations for application to shelf sea modelling. Cont. Shelf Sea Res. 2, 243–254.

Bleck, R., Boudra, D., 1986. Wind-driven spin-up in eddy-resolving ocean models formulated in isopycnic and isobaric coordinates. J. Geophys. Res. 91, 7611–7621.

Bryan, K., 1969. A numerical method for the study of the circulation of the world ocean. J. Comput. Phys. 4, 347–376.

Chippada, S., Dawson, C., Wheeler, M., 1998. A godonov-type finite volume method for the system of shallow water equations. Comput. Methods Appl. Mech. Eng. 151, 105–130.

Deleersnijder, E., Beckers, J., 1992. On the use of the σ-coordinate system in regions of large bathymetric variations. J. Mar. Sys. 3, 381–390.

Deleersnijder, E., Ruddick, K., 1992. A generalized vertical coordinate for 3D marine problems. Bull. Soc. R. Sci. Liège 61, 486–502.

Ferziger, J., Perić, M., 1995. Computational methods for fluid dynamics. Springer, New York.

Leendertse, J., 1967. Aspects of a computational model for long water wave propagation, Memorandum RH-5299-RR. Rand Corporation, Santa Monica.

Leendertse, J., Liu , S., 1978. A three-dimensional turbulent energy model for non-homogeneous estuaries and coastal sea systems. In: Nihoul, J. (Ed.), Hydrodynamics of Estuaries and Fjords. Elsevier, Amsterdam, pp. 387–405.

Levitus, B., 1982. Climatological atlas for the world ocean, NOAA Prog. Papers 13. US Government Printing Office, Washington DC.

Martins, F., Neves, R., Leitão, P., 1998. A three-dimensional hydrodynamic model with generic vertical coordinate. In: Babovic, V., Larsen, L. (Eds.), Proceedings of Hydroinformatics'98, Vol. 2. Balkema, Rotterdam, pp. 1403–1410.

Mellor, G., Blumberg , F., 1985. Modeling vertical and horizontal diffusivities with the sigma coordinate system. Mon. Wea. Rev. 113, 1379–1383.

Neves, R., 1985. Étude expérimentale et modélisation mathématique des circulations transitoire et résiduelle dans l'estuaire du Sado, PhD thesis. Université de Liège, Liège.

Oberhuber, J., 1993. Simulation of the Atlantic circulation with a coupled Sea Ice – Mixed Layer – isopycnal general circulation model, 1, model description. J. Phys. Oceanogr. 23, 830–845.

Phillips, N., 1957. A coordinate system having some special advantages for numerical forecasting. J. Meteorol. 14, 184–185.

Ribeiro, M., Neves, R., 1982. Caracterização hidrográfica do estuário do Sado, Tech. Report. Dep, Engenharia Mecânica, I.S.T.. Universidade Técnica de Lisboa, Lisbon.

Rodrigues, A., 1992. Environmental status of a multiple use estuary, through the analysis of benthic communities: the Sado estuary, Portugal, PhD Thesis. University of Stirling, Stirling.

Santos, A., 1995. Modelo hidrodinâmico tridimensional de circulação oceânica e estuarina, PhD thesis. I.S.T.. Universidade Técnica de Lisboa,, Lisbon.

Sobral, J., 1977. Estuário do Sado Observação de correntes de marés, Tech. Report. Instituto Hidrográfico, Lisbon.

Vale, C., Sundby, B., 1987. Suspended sediment fluctuations in the Sado estuary on semi-diurnal and fortnightly time scales. Estuar. Coast. shelf sci. 25, 495–508.

Vinokur, M., 1989. An analysis of finite-difference and finite-volume formulations of conservation laws. J. Comput. Phys. 81, 1–52.

Wollast, R., 1978. Rio Sado, campagne de mesures de juillet1978 Tech. Report. Secretaria de estado do ambiente, Lisbon.

Wollast, R., 1979. Rio Sado, campagne de mesures d'avril1979, Tech. Report. Secretaria de estado do ambiente, Lisbon.